Available online at www.sciencedirect.com

ScienceDirect

Procedia CIRP 117 (2023) 145–150

www.elsevier.com/locate/procedia

19th CIRP Conference on Modeling of Machining Operations

Battery Tray Fixture Stiffness and Damping Modeling for Surface Quality Prediction

Marc Raffestin[a,b], Cyrille Urville[b], Philippe Lorong[a], Mikhaïl Guskov[a]

[a]*Laboratoire PIMM, Arts et Metiers Institute of Technology, CNRS, Cnam, HESAM Universite, 151 boulevard de l'Hopital, 75013 Paris (France)*
[b]*PCI SCEMM, Rue Copernic, 42030 Saint-Etienne Cedex 2 (France)*

* Corresponding author. Tel.: +33-6-15-58-44-46 ; *E-mail address:* marc.raffestin@pci.fr

Abstract

Energetic transition in automotive industry leads to production of new parts such as battery trays. These parts present machining challenges linked to their vibration. It was shown that dynamic model accuracy is highly conditioned by fixture modeling. In the present work a clamping modeling approach for machining simulation is presented. Updating methodology of fixture stiffness and damping, based on dynamic reduction, is detailed. It allows to assess the influence of fixture on part dynamic behaviour in machining. Numerical predictions of machined surface geometry are compared to experiments on a battery tray part.

Keywords: fixture modeling; fixture damping; fixture stiffness; dynamic reduction; machining simulation; flexible part machining

1. Introduction

Nowadays a major energetic transition takes place in the automotive sector. This leads to the design of lighter and more optimized parts, the machining of which can be particularly tricky. The dimensioning of the machining operations for this type of part can benefit from a better understanding of the physical phenomena present during the machining and in particular concerning the vibratory aspects. A good example is battery tray part, which is composed of several aluminium-extruded profiles assembled [1]. These lightweight, large-dimensions, thin-walled components could presented major vibrations challenges during machining. Thus, it is important to find good process conditions in agreement with these constraints at earlier design step. Numerical simulation is a useful tool to determine a virtual model of the vibrational behaviour of the part. The objective is then to build a virtual model sufficiently representative of reality. Finite element (FE) method enable to create highly representative model of the part without attachment considering its free-free eigenmodes. The prediction of the dynamic behavior of assemblies, including thus contacts between different bodies, is however more delicate in particular when one seeks to predict the levels of damping. For a monolithic part, the modal damping ratios are close 0.01% whereas, for a clamped part, depending on the modes, the damping ratios can vary from 0.1% to 5% [2]. Several approaches exist to predict contact behaviour more specifically as a damping source [3, 4, 5]. In this context, it became interesting to define a strategy to model the clamped part behaviour through the development of fixture models [6, 7]. The final clamping model need to be as simple as possible for industrial automation of re-calibration and use.

The aim of this work is to analyse the capacity of a simple fixture modelisation to represent the experimental contribution of fixture on part dynamic behaviour, especially to predict modal damping and part behaviour during machining. The used modelisation includes stiffness and damping parameters updated so that the virtual model best reproduces the measurements. This update uses a reduced model in order to minimize calculation costs by avoiding modal analyzes on the complete FE model. Finally a face milling operation is used to compare simulation and experiments and analyse modelisation capacities to predict machined surface quality and vibrations during machining.

Experimental modal analysis of the clamped part is presented in section 2. The fixture modelling approach is described in section 3. The reduced model used to update de FE model is presented in section 4. Updating method is presented in section 5 and a discussion is provided in section 6. A battery tray profile machining operation, detailed in section 7, is used to

2212-8271
10.1016/j.procir.2023.03.026

compare experiments with simulations. These results are presented in section 8 before a general conclusion in section 9.

2. Experimental modal analysis

The part under consideration is a battery tray element, constituted by an extruded profile of 400mm length. Its thin-walled shape, see Figure 1, makes it subject to vibration during machining. The defects observed on flexible machined surfaces generally come from the first modes of vibrations because they contribute the most to the relative motion of the part with respect to the tool. In this document we will thus focus on the first 9 modes which are included in the range [200Hz, 1600Hz].

Two Kistler accelerometers (ref. 8776B100S) are used for experimental modal analysis. The placement of theses sensors and the choice of the localization of PCB hammer (ref. 086C02) impacts, see Figure 1, are determined using algorithm detailed in [8] and implemented in SDTools software [9].

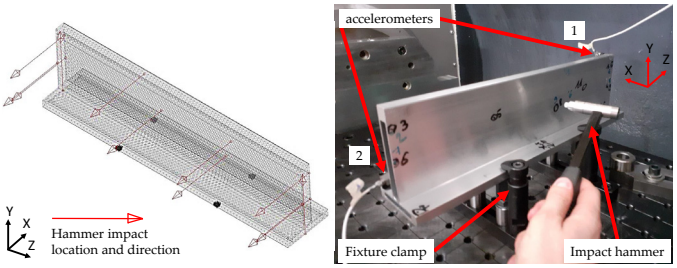

Figure 1: Experimental modal analysis configuration: sensors placements (left) and hammer testing (right)

The frequency response functions (FRF) of the system are then extracted to perform a parametric identification of poles-residues model. These experimental modal data, namely eigenfrequencies ω_i^x, damping ratios ξ_i^x, and corresponding modal shapes $\underline{\phi}_i^x$ (on sensors and impacts locations), are used as references for further model updating. These data are summarized in Table 1 and Table 2.

3. Clamping model – Clamping parameters

The part is held by 4 screwed clamps (Norelem ref 04371). The size of the contact between these clamps and the part is quite small with respect to the size of the part or the size of the wavelength of the first eigenmodes. Thus, as in [7], we have chosen to model these contact areas by small rigid surfaces. A master node is linked to each of these 4 surfaces. A 6 degrees of freedom (DOF) grounded viscoelastic spring is used to represent global stiffness and damping of both contact and fixture element for each clamping zone (see Figure 2 for normal direction). As clamping zones are similar, all Kelvin-Voigt models are considered as identical. Six parameters are considered to define the stiffnesses of each spring: normal stiffness K_{Ty}, shearing stiffnesses K_{Tx} and K_{Tz}, torsion stiffness K_{Ry}, bending stiffnesses K_{Rx} and K_{Rz}; six damping parameters are equivalently represented by normal damping C_{Ty}, shearing damping C_{Tx} and C_{Tz}, torsion damping C_{Ry}, bending damping C_{Rx} and C_{Rz}.

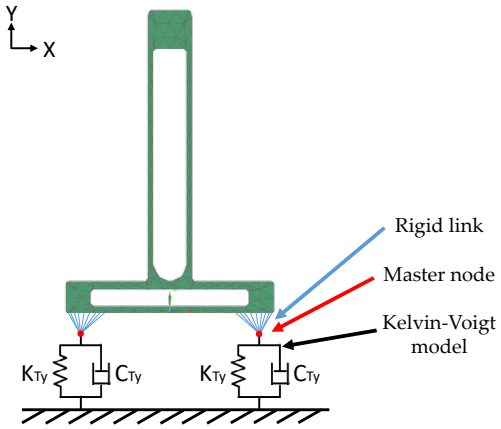

Figure 2: Fixture modeling – Normal direction

4. Reduced model construction

A finite element (FE) model of the clamped workpiece is used to compute a Ritz basis in which the updating process is carried out. Used initial values for clamping stiffness parameters are those obtained in [7]. The workpiece is modeled with 183 600 T10 elements, leading to $n = 1\,674\,414$ DOF.

A Mac-Neal type approach [10, 11] is used to construct the initial Ritz basis. In this approach, a set of n_D eigenmodes $\underline{\underline{{}^D\phi}} = \left[{}^D\underline{\phi}^1, ..., {}^D\underline{\phi}^{n_D}\right]$ is enriched by a set of n_S static deformed shapes $\underline{\underline{{}^S\phi}} = \left[{}^S\underline{\phi}^1, ..., {}^S\underline{\phi}^{n_S}\right]$ generated by unit loads on each DOF of master nodes (see Figure 3).

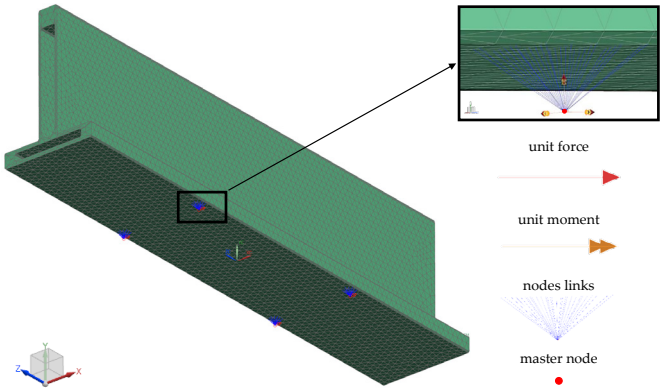

Figure 3: Unitary forces and moments used for the Mac-Neal approach

The subsequent Ritz basis $\underline{\underline{T}} = \left[{}^D\underline{\underline{\phi}}, {}^S\underline{\underline{\phi}}\right]$ totals $n_R = n_D + n_S$ components. After orthogonalization and normalization with respect to the global FE mass matrix this basis is then noted ${}^{(1)}\underline{\underline{T}}$. Let $\underline{\underline{M}}$ and $\underline{\underline{K}}$ be the mass matrix and the stiffness matrix respectively of the full FE model. The associated reduced mass

and stiffness matrices are defined as: $\underline{\underline{\tilde{M}}} = {}^{(1)}\underline{\underline{T}}^T \underline{\underline{M}} \, {}^{(1)}\underline{\underline{T}}$ and $\underline{\underline{\tilde{K}}} = {}^{(1)}\underline{\underline{T}}^T \underline{\underline{K}} \, {}^{(1)}\underline{\underline{T}}$.

5. Updating clamping parameters

5.1. Stiffness parameters

Let Δk_j, for $j = 1$ to 6, be the parameters representing the correction to apply on clamping stiffness parameters to minimize the gap $\Delta\omega$ between measured eigenfrequencies ω_i^x and simulated ones ω_i^y: $\Delta\omega = \sum_i^{n_r} |\omega_i^x - \omega_i^y|$. This gap must apply on paired eigenmodes, meaning that their MAC (Modal assurance criterion [12]) is close to 1. Thus, n_r may be lower than the number of found experimental eigenmodes. As shown on Figure 4, after Δk_i optimization, the MAC matrix is close to be diagonal and, for example, for the 6 first eigenmodes the MAC is greater than 0.95.

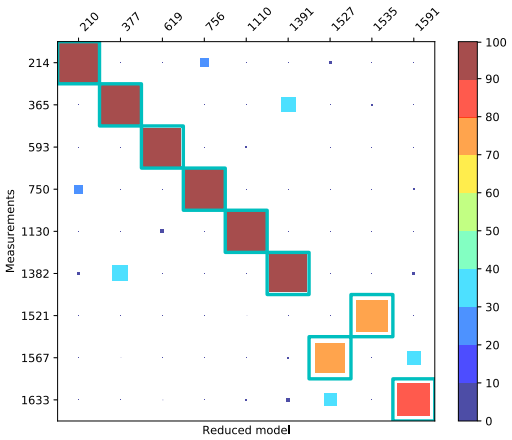

Figure 4: MAC matrix reduced model vs experiment

For reasons of numerical efficiency it is important to avoid solving an eigenvalue problem on the full FE model for each set Δk_i tested. The Ritz basis ${}^{(1)}\underline{\underline{T}}$ is thus used and it is then possible to solve the following reduced eigenvalue problem:

$$\left[\underline{\underline{\tilde{K}}} + \underline{\underline{\tilde{\Delta k}}} - \lambda \underline{\underline{\tilde{M}}}\right] \underline{\alpha} = \underline{0} \tag{1}$$

where $\underline{\underline{\tilde{\Delta k}}} = \sum_{j=1}^{6} \Delta k_j \left({}^{(1)}\underline{\underline{T}}^T . \underline{\underline{\hat{K}}}_j . {}^{(1)}\underline{\underline{T}} \right) = \sum_{j=1}^{n_j} \Delta k_j \underline{\underline{\tilde{K}}}_j$. Each pattern matrice $\underline{\underline{\hat{K}}}_j$ corresponds to the full FE stiffness matrix associated solely to the 4 springs (clamping) with $\Delta k_i = \delta_{ij}$ (Kronecker symbol).

The eigenvectors computed from (1) give place to the new Ritz basis ${}^{(2)}\underline{\underline{T}}$ based on a selection of $n_r \leq n_R$ paired modes corresponding to low eigenfrequencies:

$${}^{(2)}\underline{\underline{T}} = {}^{(1)}\underline{\underline{T}} . \underline{\alpha} = \left[{}^{(2)}\underline{\phi}_1, \ldots, {}^{(2)}\underline{\phi}_{n_r} \right], \quad \underline{\alpha} = \left[\underline{\alpha}_1, \ldots, \underline{\alpha}_{n_r} \right] \tag{2}$$

The shapes of ${}^{(2)}\underline{\underline{T}}$ eigenmodes obtained after optimization are plotted on Figure 5. The stiffness updating (identification of Δk_j), when performed automatically in a least-squares optimization, is subject to multiple local minima. It does not ensure a balanced discrepancy, inducing thus errors on some of the eigenmodes. A manually driven iterative approach was carried out instead. It proceeds in 2 steps. A first approximation of Δk_j values is sought, ensuring that all the mode shapes are paired. Then a second optimization, consisting in sequential Δk_j adjustment one after another, minimizing the eigenfrequency discrepancy $\Delta\omega$.

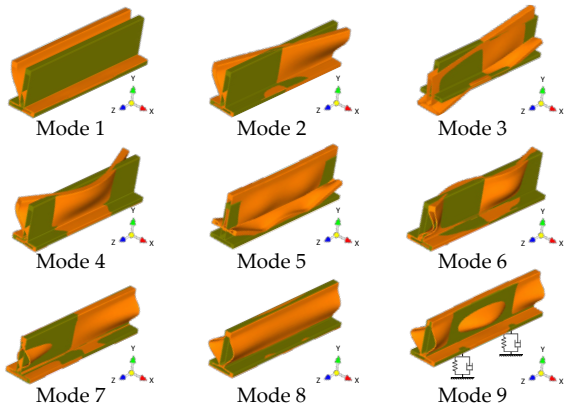

Figure 5: Numerical modal shapes (green – undeformed, orange – eigenmode)

5.2. Damping parameters

Global damping matrix could be expressed as :

$$\underline{\underline{C}} = \sum_{l=1}^{nl} c_l \underline{\underline{\hat{C}}}_l \tag{3}$$

where $\underline{\underline{\hat{C}}}_j$ is a unit damping application pattern, analogous to $\underline{\underline{\hat{K}}}_j$, and c_l are damping parameters. These parameters are to be optimized in order to minimise difference $\Delta\xi$ between measured modal damping ratios ξ_i^x and numerical ones ξ_i^y: $\Delta\xi = \sum_i^{n_r} |\xi_i^x - \xi_i^y|$. Modal damping ξ_i^y, associated to the i^{th} paired eigenmode, can be defined by $2\omega_i^y \xi_i^y = {}^{(2)}\underline{\phi}_i^T . \underline{\underline{C}} . {}^{(2)}\underline{\phi}_i$.

For reasons similar to those above mentioned (automated optimization tending to converge to an ill-distributed discrepancy or to negative damping ratios), the identification process was

carried out manually, guided by the use of sensitivities:

$$\frac{\partial \xi_i^v}{\partial c_j} = \frac{1}{2\omega_i^v} {}^{(2)}\underline{\phi}_i^T \cdot \underline{\underline{\hat{C}}}_j \cdot {}^{(2)}\underline{\phi}_i. \quad (4)$$

These sensitivities are given in Table 3. For each row, the sensitivities are normalized by the maximum sensitivity.

6. Updating results and discussion

Based on approach presented in subsection 5.1, the following set of stiffness values is deduced: $K_{Tx} = K_{Tz} = 500$kN/mm, $K_{Ty} = 50\,000$kN/mm, $K_{Rx} = 1$kNm/rad, $K_{Ry} = 9$kNm/rad and $K_{Rz} = 175$kNm/rad. Subsequent relative frequencies errors are given in Table 1. The difference between K_{Rx} and K_{Rz} are due to clamping system asymmetry as it could be seen on Figure 1. The modes 7 to 9 are thin wall modes with low displacement on sensors locations inducing lower MAC values (Figure 4). Modes 7 and 8 are individual thin wall bending modes.

Table 1: Eigenfrequencies: Experimental vs Numerical

Mode number	Experimental frequency (Hz)	Numerical frequency (Hz)	frequency relative error
1	214	210	-1.83 %
2	365	377	3.36 %
3	593	619	4.41 %
4	750	756	0.76 %
5	1130	1110	-1.75 %
6	1382	1391	0.62 %
7	1521	1527	0.91 %
8	1567	1535	-2.59 %
9	1633	1591	-2.57 %

Concerning fixture damping identification, once the mode sensitivities are evaluated (Table 3), a manual iteration process led to the following damping values: $C_{Tx} = 263$kNs/mm, $C_{Ty} = 62\,600$kNs/mm, $C_{Tz} = 375$kNs/mm, $C_{Rx} = 73.21$mNms/rad, $C_{Ry} = 4.50$Nms/rad and $C_{Rz} = 256.67$Nms/rad. Relative modal damping ratios errors are given in Table 2.

The highest error is obtained for the 5^{th} mode. The shape of the 5^{th} mode near to the contact zone induces internal bending within clamping area. The initial assumption of rigid surfaces induced by small contact zone appears less valid for this mode. Our current analysis is that this internal flexion might not be well represented by a combination of global rigid translation and rotation and thus lead to poor representation of contact contribution to modal damping.

The estimation fo the modal damping of the 1^{st} mode is nearly 8.5 times lower than the measured value. The nodal displacement of master nodes for this mode are concentrated on a single degree of freedom: shearing along X axis. This induces a high dependency to C_{Tx} damping parameter. However, C_{Tx} is also implicated in updating of most of other modal damping ratios. Table 3 highlights dominance of C_{Tx} for mode 1 and interdependence of this parameter for other modes. The Table 3 presented the C_i contribution to damping ratios normalized by modes which highlight dominance of C_{Tx} for mode 1 and interdependence of this parameter for many other modes (modes 2, 3, 5, 6, 7 and 8).

Table 2: Modal damping ratios: Experimental vs Numerical

Mode number	ξ^x (%)	ξ^v (%)	ξ relative error
1	0.194	0.023	-87.9 %
2	0.202	0.301	48.5 %
3	0.644	0.767	19.0 %
4	0.039	0.054	38.0 %
5	0.320	0.808	152.6 %
6	0.129	0.066	-49.4 %
7	0.360	0.510	-41.8 %
8	0.286	0.324	13.4 %
9	0.352	0.157	-55.5 %

For all other modes, modal damping error is at most around 50% at maximum and aim to represent really low values of damping ratios. A way to improve this is to optimise damping during stiffness optimisation, thus enabling to take into account flexibility variation within the contact that could help to find better set of parameters to represent experimental clamping behaviour. Another improvement could be to add a more detailed model for clamps and supports in order to update only contact stiffness and damping and take into account proper damping of fixture components.

7. Machining experiment and simulation

Here a face milling operation is considered. The tool path was defined in order to observe a transition from stable cutting to chatter. The cutter is an insert mill (MAPAL ref. 30545058, inserts ref. 30559594) with feed rate of 0.5 mm/rev, cutting depth 1mm and rotation speed of 18000 rev/min. These cutting conditions come from an industrial case. The part is held by screwed clamps (Norelem ref 04371), tightened to 9N.m on supports (Norelem ref 02040). The supports are located at 120 mm from the part side in length direction and 5mm from the X axis sides. Experimental data extracted from this study case are metrological measures of the machined surface. The 4 measured zones are presented on Figure 6.

The simulation of this machining operation is done with the *nessy2m* software [13]. The used time domain approach involves the following ingredients: an evolutive geometrical model of the machined surface allowing to follow material erasing by each teeth, a part FE dynamical model based on ${}^{(2)}\underline{\underline{T}}$ Ritz basis, and a line force tool-workpiece interaction model for cutting forces evaluation (cutting law): $F_i = k_i h + K_{0i}$, with h the uncut chip thickness and i the component of the force vector. This vector is expressed in (n,e,c) basis where n is the local normal of the rake face, e is a local tangent to the cutting edge and c is defined in order to have a orthonormal basis. The cutting force model lead to force amplitude of resultant in the order of magnitude of 60N if no vibration occurred.

Table 3: Normalized contribution to modal damping for each damping parameter and for each eigenmode

Damping parameters	Mode 1	Mode 2	Mode 3	Mode 4	Mode 5	Mode 6	Mode 7	Mode 8	Mode 9
C_{Tx}	1.000	0.786	0.456	0.021	0.924	0.463	0.635	0.524	0.038
C_{Ty}	0.050	0.000	0.252	0.000	0.700	0.015	0.002	0.015	0.041
C_{Tz}	0.032	0.551	0.562	0.383	1.000	1.000	0.668	0.812	1.000
C_{Rx}	0.000	0.060	1.000	0.702	0.005	0.149	0.043	0.030	0.024
C_{Ry}	0.000	0.047	0.001	1.000	0.009	0.164	0.0284	0.041	0.024
C_{Rz}	0.005	1.000	0.006	0.553	0.019	0.075	1.000	1.000	0.031

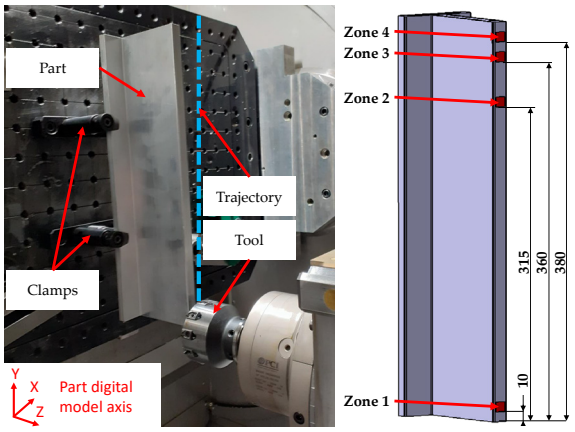

Figure 6: Experimental (left) and metrological (right) setup

Two cases are simulated. The first one takes into account the updated stiffnesses with experimentally measured modal damping ratios ξ_i^x. The aim of this simulation is to be the numerical reference. The second one, based on ω_i^v and ξ_i^v, corresponds to updated stiffnesses and damping ratios (respectively k_j and c_j), aims to analyse the impact of damping prediction errors on machining simulation, particularly on vibrations.

8. Machining Results and discussion

Figure 7 presents the experimental surfaces extraction on the 4 measured zones while Figure 8 presents this extraction for simulated surfaces. On both figures one can see that:

- the process is initially stable and that high vibrations occurrences appear after the middle of the part,
- during zone 2 machining, vibrations make the inserts to machine again the surface with the back side of the tool,
- the previous phenomenon is not visible on zones 3 and 4 because the front side's inserts are out of the part; then cutting forces and vibrations are reduces and back side does not machine,
- individual tooth cut, due to high vibrations, can be seen on zones 2, 3 and 4,
- the measured altitudes are higher in the centre of the surface than on both sides (hat shape).

Thereby, the real machined surface and the simulated surfaces are qualitatively similar.

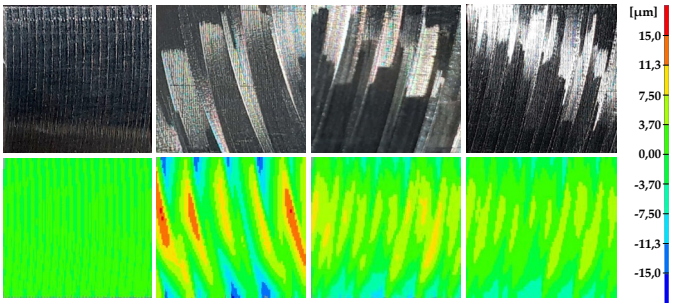

Figure 7: Local experimental flatness measurements (left to right: zone 1 to 4)

It can be noticed that vibrations pattern are identical between experiments and simulations.

However, concerning the amplitudes of variation of the altitudes, we note that the amplitudes are in the same order of magnitude for the simulation with experimental damping ratios but are four times greater for simulation with updated damping ratios. In the latter case, the simulated machining is noticeably more unstable than in reality. This confirms that the level of fidelity with which damping is reproduced in the numerical models must be taken into account.

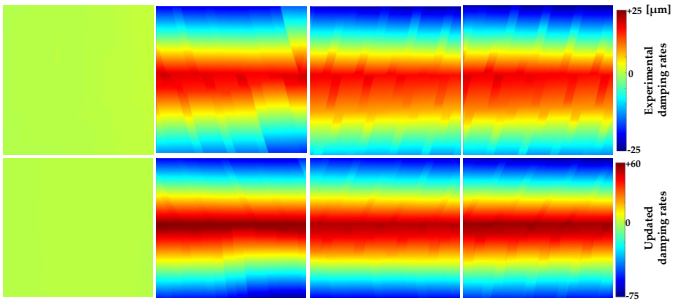

Figure 8: Local flatness numerical measurements (left to right: zone 1 to 4)

In order to go further in the comparison between reality and simulation an accelerometer (accelerometer 2 on Figure 1) was used to analyse vibration during machining. Spectrograms Figure 9 show, when vibrations initiate, which mode is concerned and with which amplitude.

Figure 9a shows that the 4th mode (750Hz) begins to vibrate significantly 2 seconds after machining starts. This aspect is reproduced by simulation (b) but not by simulation (c) where it starts after 1.25 seconds. This shows again that simulation (c) produces a more unstable machining.

Still concerning this 4th mode, we note that for simulations (b) and (c) that the vibration amplitude continues to grow after its appearance. During real machining this is not the case (stagnation of vibration amplitudes). We suspect that a ploughing effect, not taken into account in these simulations, explains this discrepancy.

Another mode observed experimentally is mode 1 (214Hz) which damping ratio is highly underestimated in the updated model (c): 0.023 instead of 0.194. This is in consistency with its exaggerated presence on spectrogram (c). A higher damping ratio should lead to postpone this apparition.

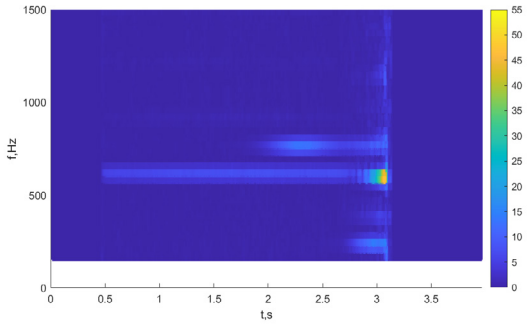

(a) experimental acceleration [unit: g]

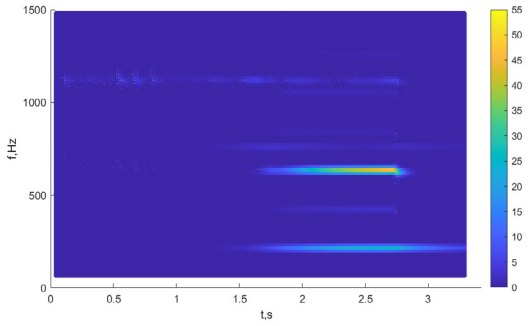

(b) numerical acceleration with experimental damping rates (ξ^x in Table 2) [unit: g]

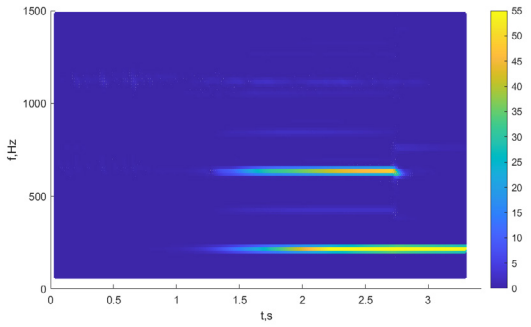

(c) numerical acceleration with updated damping rates (ξ^v in Table 2) [unit: g]

Figure 9: Experimental and numerical spectrograms

9. Conclusion

This study presented a clamping modelling methodology for machining simulation. Updated fixture stiffness and damping, based on dynamic reduction, enable to assess the influence of fixture on part dynamic behaviour in machining. First, stiffness parameters is carried out based on eigenfrequency discrepancy reduction of a selection of paired eigenmodes. Then, damping is updated based on modal damping discrepancy. Identification carried out with manual guidance based on output sensitivity matrix. Manually guided iterative updating allowed to keep the eigenfrequency and modal damping discrepancies moderate, although unevenly distributed over the set of nine modes of interest. Analysis about model and updating methodology's strengths and weaknesses are detailed. Machining case is used to compare simulation and experiments and analyse modelling capacities to predict machined surface quality and vibrations during manufacturing process. Chatter pattern and machining behaviour are observed for both numerical simulation and experimentation. Differences between numerical and experimental machining could be explained by vibration amplitudes which are dependent to numerical damping ratios estimation. Next steps are about improving fixture model by taking into account elements flexibility in order to be able to compute more accurately damping within the entire fixture elements of the system. As a further perspective, this model could be used to test influence of rotational speed which is well known to have a great influence on machining stability.

References

[1] Electric Vehicle Battery Box | AEC.
URL https://www.aec.org/page/electric-vehicle-battery-box
[2] R. N. Coppolino, Structural dynamics modeling–tales of sin and redemption, Sound & Vibration (2016) 7.
[3] L. Gaul, M. Mayer, Modeling of contact interfaces in built-up structures by zero-thickness elements, in: Conf. Proc.(CD ROM) IMAC XXVI: Conf. & Expo. on Str. Dyn, 2008.
[4] B. J. Deaner, M. S. Allen, M. J. Starr, D. J. Segalman, H. Sumali, Application of viscous and iwan modal damping models to experimental measurements from bolted structures, Journal of Vibration and Acoustics 137 (2) (2015).
[5] B. Fang, R. DeVor, S. G. Kapoor, Influence of friction damping on workpiece-fixture system dynamics and machining stability, J. Manuf. Sci. Eng. 124 (2) (2002) 226–233.
[6] L. Nguyen, H.-C. Möhring, Stiffness and Damping Properties of a Swing Clamp: Model and Experiment, Procedia CIRP 58 (2017) 299–304. doi:10.1016/j.procir.2017.03.190.
[7] S. Moussavi, M. Guskov, J. Duchemin, P. Lorong, Clamping Modeling in Automotive Flexible Workpieces Machining, Procedia CIRP 101 (2021) 134–137. doi:10.1016/j.procir.2021.04.004.
[8] E. Balmes, Orthogonal maximum sequence sensor placements algorithms for modal tests, expansion and visibility, IMAC, January 145 (2005) 146.
[9] SDTools – Product and company presentation.
URL https://www.sdtools.com/
[10] R. H. MacNeal, A hybrid method of component mode synthesis, Computers & Structures 1 (4) (1971) 581–601. doi:10.1016/0045-7949(71)90031-9.
URL https://linkinghub.elsevier.com/retrieve/pii/0045794971900319
[11] T. Rose, Using residual vectors in msc/nastran dynamic analysis to improve accuracy, in: MSC World Users' Conference, 1991, pp. 1–18.
[12] M. Pastor, M. Binda, T. Harčarik, Modal assurance criterion, Procedia Engineering 48 (2012) 543–548, modelling of Mechanical and Mechatronics Systems. doi:https://doi.org/10.1016/j.proeng.2012.09.551.
[13] G. Coffignal, P. Lorong, L. Illoul, A general method to accurately simulate material removal in virtual machining of flexible workpieces (2015).